Intermetallics 17 (2009) 17–24

Contents lists available at ScienceDirect

Intermetallics

journal homepage: www.elsevier.com/locate/intermet

Microstructure of Al_3Sc with ternary rare-earth additions

Y. Harada [a,*], D.C. Dunand [b]

[a] Advanced Manufacturing Research Institute, National Institute of Advanced Industrial Science and Technology (AIST), 1-2-1 Namiki, Tsukuba, Ibaraki 305-8564, Japan
[b] Department of Materials Science and Engineering, Northwestern University, 2220 Campus Drive, Evanston, IL 60208-3108, USA

ARTICLE INFO

Article history:
Received 9 September 2008
Accepted 11 September 2008
Available online 5 November 2008

Keywords:
A. Trialuminides
A. Rare-earth intermetallics
B. Solid-solution hardening
D. Microstructure
F. Diffraction

ABSTRACT

The microstructure of ternary $L1_2$-$Al_3(Sc_{1-y}RE_y)$ intermetallics, where RE is one of the rare-earth elements selected from five light (La, Ce, Nd, Sm or Eu) or two heavy lanthanoids (Yb or Lu), was investigated as a function of RE concentration for $0.02 \le y \le 0.75$. Alloys with light RE show two phases: $L1_2$-Al_3(Sc,RE) and $D0_{19}$-Al_3(RE,Sc) (or $C11_b$-Al_4(Eu,Sc)). Alloys with heavy RE exhibit a single $L1_2$-Al_3(Sc,RE) phase. The maximum RE solubility in the $L1_2$ phase is very low (<0.4 at.%) for La, Ce, Nd and Eu, low (3.2 at.%) for Sm and complete solid-solution for Yb and Lu. Both lattice parameter and hardness of the $L1_2$-Al_3(Sc,RE) phases increase linearly with Sm, Yb or Lu concentration, and the magnitude of both effects correlates with the atomic size mismatch between Sc and RE.

1. Introduction

The binary intermetallic compound Al_3Sc is of potential interest for high-temperature structural applications because of its low density (3.03 mg m^{-3}) given that Sc is by far the least dense of the transition metals, its relatively high melting point (1593 K) and its cubic $L1_2$ structure may provide some ductility. Polycrystalline Al_3Sc is, however, brittle at room temperature [1], so there is interest in achieving partial substitution of Sc by other elements that may increase ductility of Al_3Sc (as reported, e.g., by the addition of Cr to Al_3Ti) [2], while also decreasing the cost of the alloy. However, there is limited knowledge of the alloying behavior of Al_3Sc. We recently investigated the substitution of Sc with transition metals (TM) from Group 3 (Y), Group 4 (Ti, Zr, Hf), and Group 5 (V, Nb, Ta) [3] and found that the solubility limit in the $L1_2$-$Al_3(Sc_{1-y}TM_y)$ phase was high for Group 3 and Group 4 metals ($\sim$12.5 at.% or $y = 0.50$), but quite low for Group 5 metals (from $\sim$1.8 at.% or $y = 0.07$ for Ta to $\sim$2.7 at.% or $y = 0.11$ for V). The lattice parameter of the $L1_2$ solid-solution decreased linearly with increasing concentration of Group 4 and Group 5 metals, but increased linearly with concentration of Y (Group 3). In addition, these $L1_2$ solid-solution-strengthened $Al_3(Sc_{1-y}TM_y)$ alloys showed significantly improved creep properties as compared to binary Al_3Sc [4]. Three prior studies (summarized in Ref. [5] and with few details from experimental results) also report solubility of Y in $Al_3(Sc_{1-y}RE_y)$ at 800 °C [6] and in various rare-earth elements (RE = Gd [7], Tb, Dy, Ho, Er [6], Sm, Tm and Lu [8]), as well as the relationship between lattice parameters and RE concentration. Solubilities were high (10–25 at.% or $y = 0.40$–1) except for Sm and Gd, the two lightest elements studied (4 at.% or $y = 0.12$ and 3.8 at.% or $y = 0.15$, respectively), and all REs increased the lattice parameter of the $L1_2$ solid-solutions.

The alloying behavior of Al_3Sc is also important for the rational design of Sc-containing aluminum alloys with coherent, nano-size $L1_2$-Al_3Sc precipitates. These precipitates interact strongly with dislocations, which can increase ambient and elevated temperature strength [9–14]. This strengthening effect is enhanced by increasing the volume fraction and the lattice mismatch of the precipitates [15], which can be achieved by adding RE to Al–Sc alloys to form ternary $Al_3(Sc_{1-y}RE_y)$ precipitates. Sawtell and Morris [16] found an improvement in the tensile strength of Al–0.3Sc alloys (all compositions are given in at.%) upon 0.3 at.% additions of Gd, Ho, Er or Y. Karnesky et al. [17] found in Al–0.06Sc–0.02RE (with RE = Y, Sm, Gd, Dy, Er and Yb) that RE segregated to the core of the precipitate after aging at 300 °C. The above alloys with RE = Y, Dy, Er exhibited improved creep resistance as compared to binary Al–0.08Sc, an effect due to the increase in mismatch between precipitates and matrix upon alloying with RE. Karnesky et al. [18] and Van Dalen et al. [19] reported that precipitates formed at 300 °C in Al–0.06Sc–0.005Gd contained relatively low amounts of Gd, while those in Al–0.06Sc–0.005Yb had higher amounts of Yb.

In the present study, the microstructure and micro-hardness of ternary $Al_3(Sc_{1-y}RE_y)$ trialuminide alloys are investigated as a function of RE concentration for $0 \le y \le 0.75$, where scandium is

* Corresponding author. Tel.: +81 29 861 7169; fax: +81 29 861 7853.
E-mail address: harada.y@aist.go.jp (Y. Harada).

0966-9795/$ – see front matter © 2008 Elsevier Ltd. All rights reserved.
doi:10.1016/j.intermet.2008.09.002

stoichiometrically replaced by one of the five light REs, La, Ce, Nd, Sm or Eu (we assign here Eu to the light RE), or one of the two heavy REs, Yb or Lu.

2. Experimental procedures

Button ingots of ternary $Al_3(Sc,RE)$ were cast by non-consumable electrode arc-melting of the pure elements on a water-cooled copper hearth under a purified, argon atmosphere. A total of 21 ternary compositions were prepared with $Al_3(Sc_{1-y}RE_y)$ stoichiometry, where $y = 0.02$, 0.04 and 0.1 for RE = Ce and Nd, $y = 0.1$, 0.25 and 0.5 for La, Sm and Eu, and $y = 0.25$, 0.50 and 0.75 for Yb and Lu. Initial charges consisted of ~3 g of high-purity metals: 99.99 wt.% pure aluminum from Johnson Matthey (Ward Hill, MA), 99.94 wt.% pure scandium from Stanford Materials (San Mateo, CA), and 99.9 wt.% pure RE from Rare Metallic Co., Ltd. Re-melting of the charge was performed six times, and the button was turned over after each solidification to ensure complete homogenization of the alloy. The resulting ingots showed a weight loss of less than 1% as compared to the initial charge. Finally, the ingots were encapsulated in quartz capsules and homogenized in argon for 24 h at 1373 K for La, Ce, Nd, Sm, Eu and Lu, and for 96 h at 1123 K for Yb (the temperature was reduced due to the low incongruent melting point of 1253 K for Al_3Yb [20]).

Metallographic preparation consisted of mounting and polishing with SiC paper and 0.25 μm Al_2O_3. Energy dispersive X-ray spectroscopy (EDS) and scanning electron microscopy (SEM) were performed to obtain chemical compositions of the bulk samples and constituent phases. The volume fraction of constituent phases was evaluated from back-scattered electron images using the Genesis software (EDAX, Tokyo). The lattice parameter of the binary Al_3Sc ($a = 4.103(1)$ Å, as determined by XRD) and its composition (74.8 at.% Al–25.2 at.% Sc, as measured by wet chemical analysis) [3] were used to calibrate the EDS detector and the lattice refinements leading to elemental compositions of the ternary $Al_3(Sc,RE)$ alloys.

Portions of the homogenized ingots were pulverized and the powders, sieved to a size below 75 μm (−250 mesh), were analyzed by X-ray diffraction (XRD) using Cu K_α radiation. Lattice parameters were calculated by the least-squares method using the JADE program (Rigaku, Tokyo). The lattice parameter $a = 4.103 \pm 0.001$ Å, determined by XRD for binary $L1_2$-Al_3Sc [3], was used to calibrate all lattice parameter of samples.

Homogenized specimens were cut perpendicular to the surface of the ingot that had been in contact with the water-cooled copper hearth. After mounting and polishing, the Vickers micro-hardness of the $L1_2$ phase was measured using a 200 g load and an indentation time of 10 s, with the average of five measurements being reported.

3. Results and discussion

3.1. Microstructure

Figs. 1–3 show the microstructures of all ternary $Al_3(Sc_{1-y}RE_y)$ alloys studied here, after casting and homogenization. As shown in Fig. 1, for additions of the first three light REs (La, Ce and Nd), the alloys consist of an $L1_2$-$Al_3(Sc,RE)$ phase (dark phase) containing a interdendritic $Al_3(RE,Sc)$ phase (bright phase). The latter phase is found by XRD and EDS analyses to be $D0_{19}$-$Al_3(La_{1-y}Sc_y)$, $D0_{19}$-$Al_3(Ce_{1-y}Sc_y)$ or $D0_{19}$-$Al_3(Nd_{1-y}Sc_y)$, with $0.028 \le y \le 0.368$. The volume fraction of the $D0_{19}$ phases, which appear at both grain-boundaries or within grains, increases with increasing RE concentration.

Fig. 2 shows the microstructures of ternary $Al_3(Sc_{1-y}RE_y)$ alloys for $0.1 \le y \le 0.5$ for the last two light REs (Sm and Eu). These alloys exhibit an $L1_2$-$Al_3(Sc,RE)$ phase (dark phase) with a second phase (bright phase) determined to be $D0_{19}$-$Al_3(Sm_{1-y}Sc_y)$ with $0.088 \le y \le 0.112$ and $C11_b$-$Al_4(Eu_{1-y}Sc_y)$ with $0.008 \le y \le 0.02$. In the case of Eu additions, the alloys also exhibit a small volume fraction of an FCC Al-phase with 0.3% Sc in solid-solution and no measurable Eu. Thus, this Eu alloy, unlike the other pseudo-binary alloys, is in a 3-phase equilibrium field, as expected from the lack of a trialuminide phase in the Al–Eu system.

Fig. 3 displays the microstructures of ternary $Al_3(Sc_{1-y}RE_y)$ for $0.25 \le y \le 0.75$ for the two heavy REs (Yb and Lu). These alloys exhibit a single phase which is confirmed by EDS and XRD analyses to exhibit the $L1_2$ structure. Pores (~5–10 μm in size) are visible at grain-boundaries or within grains, and are most probably due to the Kirkendall effect [21]. Since Al_3Sc is incongruently melting (peritectic reaction), non-equilibrium solidification of a melt with Al_3Sc composition leads to a microstructure consisting of Al_2Sc and Al–Al_3Sc eutectic. Homogenization of the alloy to the equilibrium single-phase Al_3Sc microstructure is achieved by the reaction of Al with Al_2Sc, which produces Kirkendall porosity because of the high diffusivity of Al [21].

3.2. Solubility limits of RE in $L1_2$-Al_3Sc

The composition of the $L1_2$-$Al_3(Sc,RE)$ phase, as measured by EDS, is shown in Fig. 4 as a function of RE concentration in the $Al_3(Sc_{1-y}RE_y)$ alloys for RE = La, Sm and Yb. All values plotted in Fig. 4 are also reported in Table 1.

As illustrated for La, in Fig. 4(a) and listed in Table 1 for other light REs (Ce, Nd and Eu), the composition of Al, Sc and RE in the $L1_2$ phase remains near constant with increasing RE additions to the $Al_3(Sc_{1-y}RE_y)$ alloys. For Sm, however, Fig. 4(b) shows that a decrease in Sc content in the $L1_2$ phase is associated with an increase in Sm content for $y \le 0.1$, with the Al content remaining constant. As shown in Figs. 1 and 2, for these five light RE additions, the $D0_{19}$ or $C11_b$ phase appears already at the lowest RE content used here ($y = 0.02$ for Ce or Nd and $y = 0.1$ for La, Sm or Eu), indicating that the solubility limit of RE in the $L1_2$ phase has been exceeded. In contrast, for the two heavy REs (illustrated in Fig. 4(c) for Yb and listed in Table 1 for Lu), the composition of the $L1_2$ phase shows a decrease in Sc which is compensated by an increase in RE level, while the Al concentration remains constant. Thus, for the $Al_3(Sc_{1-y}Yb_y)$ and $Al_3(Sc_{1-y}Lu_y)$ alloys, the two REs are fully soluble up to the highest concentration studied here ($y = 0.75$) and replace Sc in the $L1_2$ phase. Ref. [8] also reported Lu to be fully soluble in $L1_2$-$Al_3(Sc_{1-y}Lu_y)$, but without listing the series of alloys used to reach this conclusion.

Fig. 5 summarizes the solid solubilities of REs in Al_3Sc and the extent of two-phase fields in the pseudo-binary systems, together with data for the other heavy REs from Refs. [6–8]. In the case of the first three light REs studied here (La, Ce, and Nd), the solubility limit in the $L1_2$ phase is very limited: ~0.1 at.% for La and Ce (i.e., $Al_3(Sc_{0.996}La_{0.004})$ and $Al_3(Sc_{0.996}Ce_{0.004})$) and 0.4 at.% for Nd (i.e., $Al_3(Sc_{0.984}Nd_{0.016})$). For Sm, the fourth light RE studied here, the solubility in the $L1_2$ phase reaches 3.2 at.% (i.e., $Al_3(Sc_{0.872}Sm_{0.128})$), in good agreement with a value of 3% given by Ref. [8]. The last light RE, Eu, is not shown completely in Fig. 5, because the trialuminide Al_3Eu does not exist; as expected the solubility of Eu in $L1_2$-Al_3Sc is quite low at 0.4 at.% Eu (i.e., $Al_3(Sc_{0.984}Eu_{0.016})$).

Conversely, the solubility limits of Sc in the Al_3RE $D0_{19}$ phases are 1.0 at.% Sc in $Al_3(La_{0.96}Sc_{0.04})$, 7.2 at.% Sc in $Al_3(Ce_{0.712}Sc_{0.288})$, 9.2 at.% Sc in $Al_3(Nd_{0.632}Sc_{0.368})$, and 2.8 at.% Sc in $Al_3(Sm_{0.888}Sc_{0.112})$, the latter value being in good agreement with a value of 2.5% given by Ref. [8]; in the $C11_b$-$Al_4(Eu_{0.98}Sc_{0.02})$, the solubility limits of Sc is 0.5 at.%. Also shown in Fig. 5 are the solubility data for the heavy REs [6–8]: with increasing atomic number from Tb to Ho, the solubility increases until complete solubility is reached for the four heaviest REs (Er, Tm, Yb and Lu), the last two of which

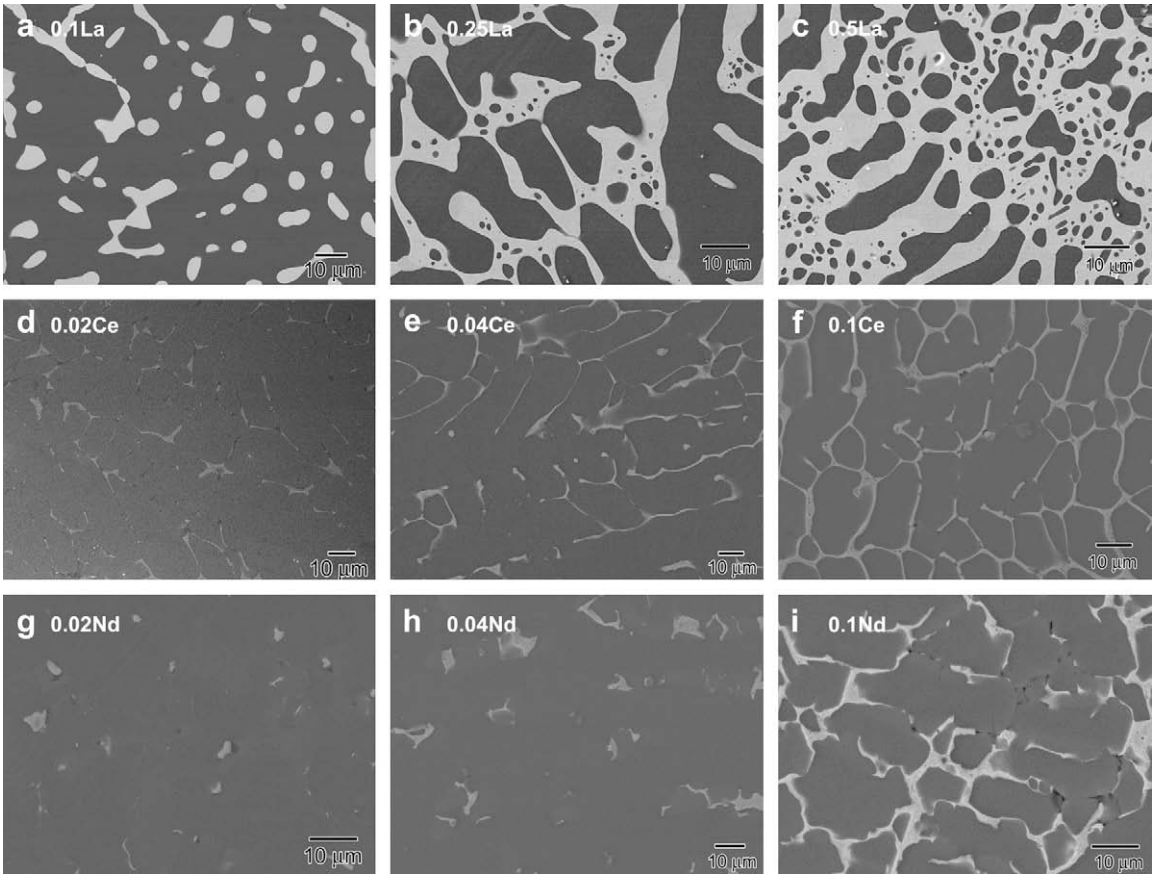

Fig. 1. SEM images of $Al_3(Sc_{1-y}RE_y)$ alloys, with RE as (a–c) La for $y = 0.1, 0.25, 0.5$; (d–f) Ce for $y = 0.02, 0.04, 0.1$; and (g–i) Nd for $y = 0.02, 0.04, 0.1$. $L1_2$-Al_3(Sc,RE) phase is dark and $D0_{19}$-Al_3(RE,Sc) phase is bright.

were also studied here. Table 1 summarizes the lattice parameters and the EDS compositional analyses of the phases for the 21 ternary alloys studied here. From the measured phase compositions, the phase volume fractions were calculated by mass conservation. Reasonable agreement was found with values determined independently from image analysis of micrographs (Figs. 1–3).

As shown in Fig. 6, RE solid-solubility in the $L1_2$ phase varies systematically with the atomic number: the light REs show little (La, Ce and Nd) or moderate (Sm and Gd) solubility, while the heavy

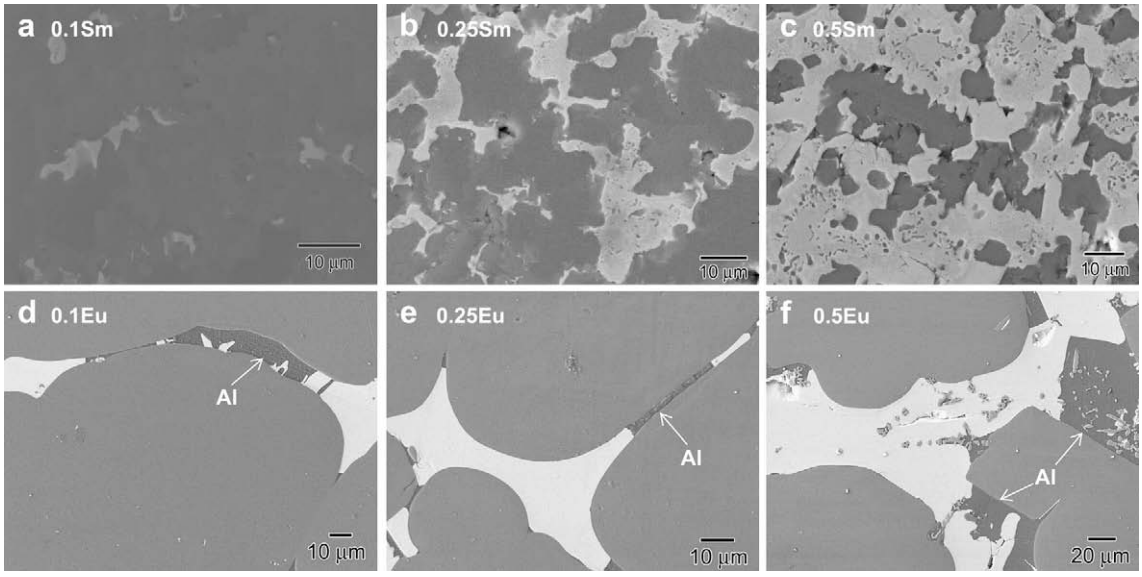

Fig. 2. SEM images of $Al_3(Sc_{1-y}RE_y)$ alloys, with RE as (a–c) Sm; and (d–f) Eu for $y = 0.1, 0.25, 0.5$. $L1_2$-Al_3(Sc,RE) phase is dark and $D0_{19}$-Al_3(Sm, Sc) and $C11_b$-Al_4(Eu,Sc) phases are bright. Al phase is shown with arrows.

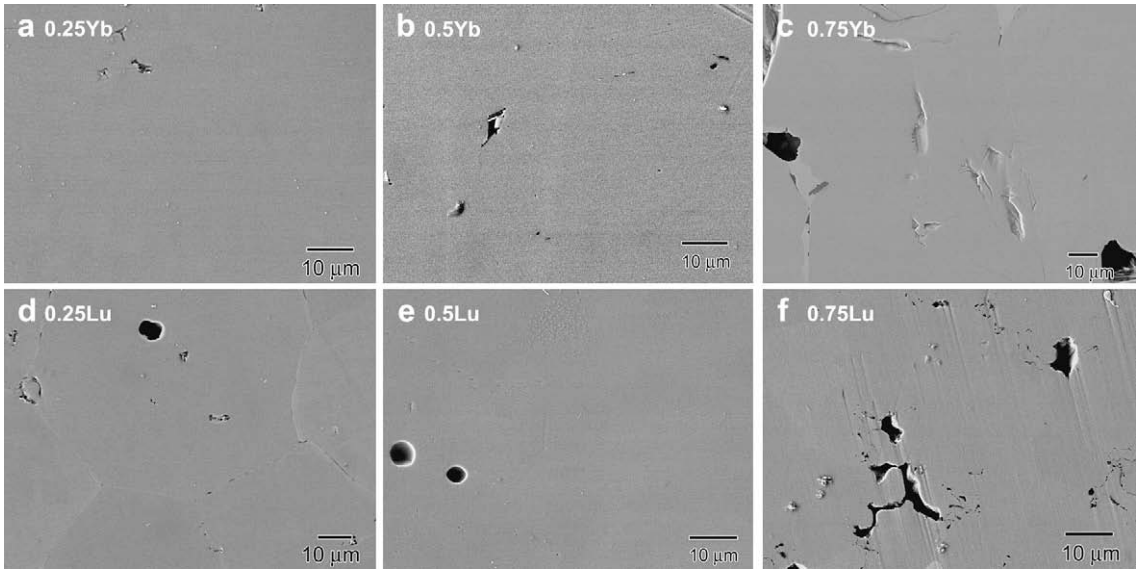

Fig. 3. SEM images of $Al_3(Sc_{1-y}RE_y)$ alloys, with RE as (a–c) Yb; and (d–f) Lu for $y = 0.25$, 0.5, 0.75. A single $L1_2$-Al_3(Sc,RE) phase is present.

REs show extensive (Tb, Dy, Ho) to complete (Er, Tm, Yb and Lu) solubility in Al_3Sc. As pointed out by Sawtell and Morris [16], this solubility trend correlates with the trend of decreasing RE metallic radius with increasing atomic number . No data exist for Pr, but based on these trends, Pr solubility in Al_3Sc is expected to be low and similar to those of Ce and Nd (and the solubility of Sc in $D0_{19}$-Al_3Pr is also expected to be quite high, as for the solubility of Sc in $D0_{19}$-Al_3Ce and $D0_{19}$-Al_3Nd).

3.3. Effect of Sc substitution by RE on lattice parameter of Al_3Sc

Fig. 6(a) and (b) shows the lattice parameter of the $L1_2$ phase (as measured by XRD) plotted against the RE concentration in the $L1_2$ phase (as measured by EDS) for the seven REs studied here (La, Ce, Nd, Sm, Eu, Yb and Lu) and for six other REs (Gd, Tb, Dy, Ho, Er and Tm) from literature data [6–8]. For Sm and the two heavy REs (Yb and Lu) studied here, a linear relationship between lattice parameter and RE concentration in Al_3(Sc,RE) exists (Fig. 6(b)), as expected from Vegard's law [23]. If the lattice parameters for binary Al_3Yb and Al_3Lu from literature [20,22] are considered, then a strong deviation from linearity is observed. It is unknown whether this is a true deviation from Vegard's law or whether experimental errors are responsible. Also plotted in Fig. 6(b) are the single data points corresponding to the maximum solubility of the other heavy REs (Gd, Tb, Dy, Ho, Er and Tm) from literature [6–8], with dashed straight lines connecting them with the origin of the graph (binary Al_3Sc). The very low solubility (<0.4 at.%) of the light REs (La, Ce, Nd and Eu) studied here prevents a clear quantification of the slope of these lines.

From the linear relationship between concentration c and lattice parameter a of the solid-solution $L1_2$-Al_3(Sc,RE) phases in Fig. 6, the best-fit slope, da/dc, is determined, corresponding to the composition dependence of $L1_2$ lattice parameter. Fig. 7 shows that these slopes for REs and those previously determined for transition-metal additions [3] correlate reasonably well with the relative atomic radius mismatch, $dR/R = (R_X - R_{Sc})/R_X$, where R is the metallic hard-sphere radius from Ref. [24] (no significant difference was found in the quality of the correlation when ionic Pauling's radii were used). A similar correlation was found by Yamamoto et al. [25] for the $L1_2$ quaternary phase $\{(AlMn)_3Ti\}_{(1-n)}X_n$, where X = Zr, V, Ag, or Ga. This correlation can be understood in terms of the size mismatch associated with the replacement of solvent

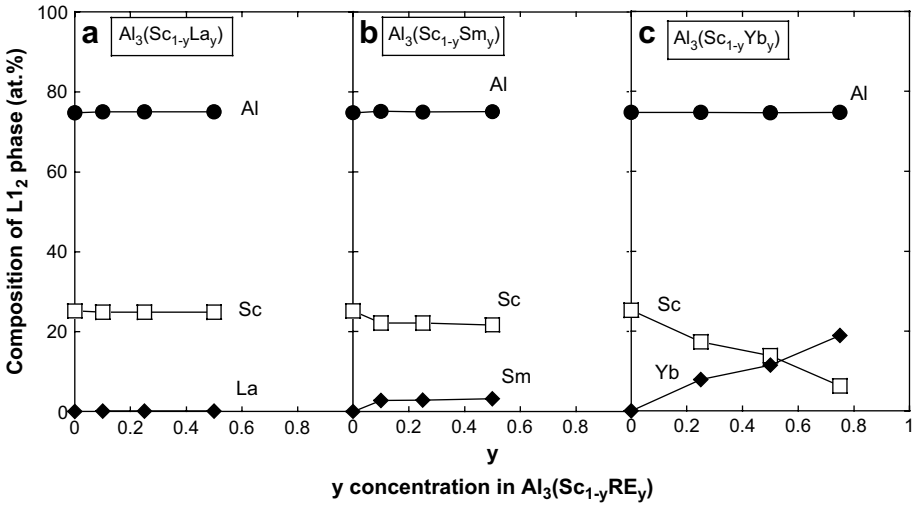

Fig. 4. Composition of the $L1_2$-Al_3(Sc,RE) phase as a function of RE concentration y in the $Al_3(Sc_{1-y}RE_y)$ alloy for RE as (a) La; (b) Sm; and (c) Yb.

Table 1
Phase composition (measured by EDS analysis) and lattice parameters (measured by XRD) for $Al_3(Sc_{1-y}RE_y)$ alloys, with RE as La, Ce, Nd, Sm, Eu, Yb and Lu.

Alloys	Structure	Chemical composition (at.%)			Volume fraction	Lattice parameter (Å)	
		Al	Sc	X	*f*	*a*	*c*
Al_3Sc [3]	$L1_2$	74.8	25.2	–	1.00	4.103 (1)	
$Al_3(Sc_{0.9}La_{0.1})$	$L1_2$	75.1 (1)	24.8 (1)	0.1 (4)	0.87 (6)	4.103 (2)	
	$D0_{19}$	74.9 (3)	1.0 (1)	24.1 (3)	0.12 (3)		
$Al_3(Sc_{0.75}La_{0.25})$	$L1_2$	75.0 (1)	24.9 (2)	0.1 (6)	0.70	4.103 (4)	
	$D0_{19}$	75.0 (3)	0.7 (1)	24.3 (3)	0.29 (9)		
$Al_3(Sc_{0.5}La_{0.5})$	$L1_2$	75.1 (2)	24.8 (2)	0.1 (2)	0.49	4.103 (3)	
	$D0_{19}$	74.9 (4)	0.9 (2)	24.2 (5)	0.51		
Al_3La [22]	$D0_{19}$	–	–	–	–	6.662	4.609
$Al_3(Sc_{0.98}Ce_{0.02})$	$L1_2$	74.9 (1)	25.0 (1)	0.1 (3)	0.96 (2)	4.103(2)	
	$D0_{19}$	75.1 (2)	4.5 (3)	20.4 (3)	0.03 (7)		
$Al_3(Sc_{0.96}Ce_{0.04})$	$L1_2$	75.0 (1)	24.9 (1)	0.1 (1)	0.90 (1)	4.103(2)	
	$D0_{19}$	75.2 (6)	7.2 (3)	17.6 (4)	0.1 (9)		
$Al_3(Sc_{0.9}Ce_{0.1})$	$L1_2$	75.2 (1)	24.7 (1)	0.1 (1)	0.83 (2)	4.103(8)	
	$D0_{19}$	75.2 (3)	7.1 (1)	17.7 (3)	0.16 (7)		
Al_3Ce [22]	$D0_{19}$	–	–	–	–	6.545	4.609
$Al_3(Sc_{0.98}Nd_{0.02})$	$L1_2$	75.1 (1)	24.6 (2)	0.3 (1)	0.97 (9)	4.105(1)	
	$D0_{19}$	75.1 (4)	5.3 (1)	19.6 (5)	0.02 (1)		
$Al_3(Sc_{0.96}Nd_{0.04})$	$L1_2$	75.0 (1)	24.7 (1)	0.3 (2)	0.95 (3)	4.106(2)	
	$D0_{19}$	75.1 (3)	7.2 (1)	17.7 (4)	0.04 (6)		
$Al_3(Sc_{0.9}Nd_{0.1})$	$L1_2$	75.0 (1)	24.6 (2)	0.4 (1)	0.85 (6)	4.106(2)	
	$D0_{19}$	75.1 (4)	9.2 (1)	15.7 (5)	0.14 (4)		
Al_3Nd [22]	$D0_{19}$	–	–	–	–	6.47	4.603
$Al_3(Sc_{0.9}Sm_{0.1})$	$L1_2$	75.1 (1)	22.1 (1)	2.8 (1)	0.92 (7)	4.117(1)	
	$D0_{19}$	75.0 (5)	2.2 (1)	22.8 (6)	0.07 (2)		
$Al_3(Sc_{0.88}Sm_{0.12})$ [8]	$L1_2$	–	–	3	–	4.114	
$Al_3(Sc_{0.75}Sm_{0.25})$	$L1_2$	75.0 (1)	22.1 (1)	2.9 (1)	0.77 (4)	4.124(1)	
	$D0_{19}$	75.2 (1)	2.4 (1)	22.4 (1)	0.22 (5)		
$Al_3(Sc_{0.5}Sm_{0.5})$	$L1_2$	75.0 (1)	21.8 (1)	3.2 (2)	0.45 (8)	4.130(1)	
	$D0_{19}$	75.1 (4)	2.8 (1)	22.1 (3)	0.54 (1)		
$Al_3(Sc_{0.1}Sm_{0.9})$ [8]	$D0_{19}$	–	2.5	–	–	6.371	4.595
Al_3Sm [22]	$D0_{19}$	–	–	–	–	6.38	4.597
$Al_3(Sc_{0.9}Eu_{0.1})$	$L1_2$	74.8 (1)	24.9 (1)	0.3 (1)	0.90(7)	4.103 (1)	
	$C11_b$	79.6 (3)	0.5 (1)	19.9 (3)	0.05(5)		
	Al	99.7	0.3	0	0.03(8)	–	
$Al_3(Sc_{0.75}Eu_{0.25})$	$L1_2$	74.7 (1)	24.9 (2)	0.4 (1)	0.83(7)	4.103 (4)	
	$C11_b$	79.6 (2)	0.5 (1)	19.9 (3)	0.13(4)		
	Al	99.7	0.3	0	0.02(9)	–	
$Al_3(Sc_{0.5}Eu_{0.5})$	$L1_2$	74.9 (1)	24.8 (2)	0.3 (1)	0.48(5)	4.103 (9)	
	$C11_b$	79.5 (2)	0.2 (1)	20.3 (2)	0.39(7)		
	Al	99.7	0.3	0	0.11(8)	–	
Al_4Eu [22]	$C11_b$	–	–	–	–	4.398	11.17
$Al_3(Sc_{0.75}Yb_{0.25})$	$L1_2$	74.8 (1)	17.3 (2)	7.9 (1)	0.98(2)	4.116 (3)	
$Al_3(Sc_{0.5}Yb_{0.5})$	$L1_2$	74.7 (2)	13.8 (4)	11.5 (2)	0.98(5)	4.131 (5)	
$Al_3(Sc_{0.25}Yb_{0.75})$	$L1_2$	74.8 (6)	6.3 (2)	18.9 (7)	0.95(3)	4.169 (3)	
Al_3Yb [20]	$L1_2$	–	–	–	–	4.204	
$Al_3(Sc_{0.75}Lu_{0.25})$	$L1_2$	74.8 (1)	17.3 (1)	7.9 (1)	0.99(2)	4.115 (1)	
$Al_3(Sc_{0.5}Lu_{0.5})$	$L1_2$	74.9 (4)	13.2 (2)	11.9 (3)	0.96(1)	4.121 (1)	
$Al_3(Sc_{0.25}Lu_{0.75})$	$L1_2$	74.7 (2)	4.8 (3)	20.5 (3)	0.95(9)	4.143 (2)	
Al_3Lu [22]	$L1_2$	–	–	–	–	4.191	
Al_3Lu [8]	$L1_2$	–	–	–	–	4.187	

atoms with solute atoms causing a distortion of the lattice. The resulting strain field may allow solute atoms to interact strongly with dislocations, thus affecting the strength of the solid-solution, as discussed in the following section.

3.4. Effect of Sc substitution by RE on micro-hardness of Al_3Sc

Fig. 8(a) and (b) shows the micro-hardness of $L1_2$-Al_3(Sc,RE) phases as a function of their RE concentration (as obtained by EDS), together with previous data for hardness of $L1_2$-Al_3(Sc,TM) with transition-metal additions (TM = Ti, Y, Zr and Hf [3]) and unalloyed binary Al_3Sc [3]. In Fig. 8(a), the maximum hardness for the $L1_2$ phases containing light REs (Ce, Nd or Eu) is relatively modest, as expected from their very low solubility in the $L1_2$ phase. A much larger hardening effect is found for La, despite its similarly very low solubility: the hardest $L1_2$ composition $Al_3(Sc_{0.996}La_{0.004})$ is more than three times as hard as binary Al_3Sc. However, the presence of finely dispersed $D0_{19}$-Al_3La within the $L1_2$ phase may be the reason for this anomalous hardness increase. As shown in Fig. 8(b), Sm with a moderate solubility (3.2 at.%), and the two heavy REs (Yb and Lu) with full solubility and transition metals (Ti, Y, Zr or Hf) with a large solubility (11.5–12.8 at.%) in Al_3Sc, show a linear hardness

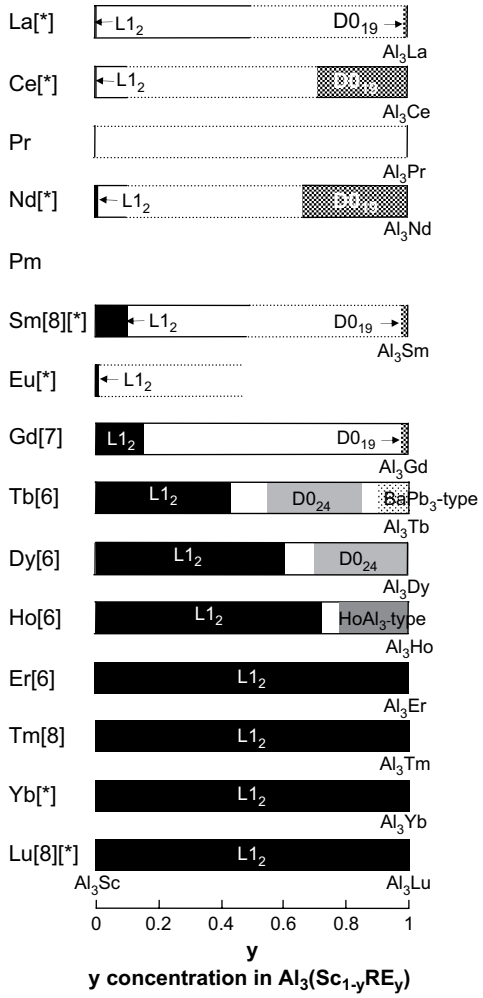

Fig. 5. Pseudo-binary Al_3Sc–Al_3RE plots showing solid solubilities of RE in the $L1_2$-Al_3(Sc,RE) phase and of Sc in various non-$L1_2$-Al_3(RE,Sc) phases, and approximate extent of two-phase fields (in white). Data are from the present investigation (labeled with [*]) and from prior literature [6–8].

increase with RE content, with hardness doubling from Al_3Sc to $Al_3(Sc_{0.25}RE_{0.75})$ for RE = Yb or Lu and to $Al_3(Sc_{0.5}Y_{0.5})$. By contrast, alloying effects for Al_3Sc on hardness are near zero for Zr and Hf and moderate for Ti and Sm, due for the latter element to its limited solubility.

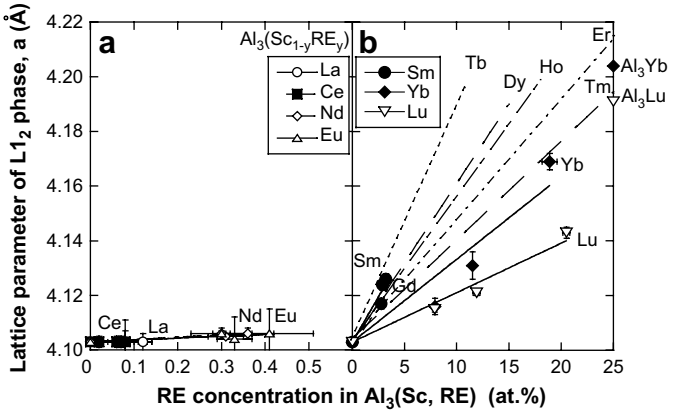

Fig. 6. Lattice parameter of the $L1_2$-Al_3(Sc,RE) phase as a function of RE concentration in that phase.

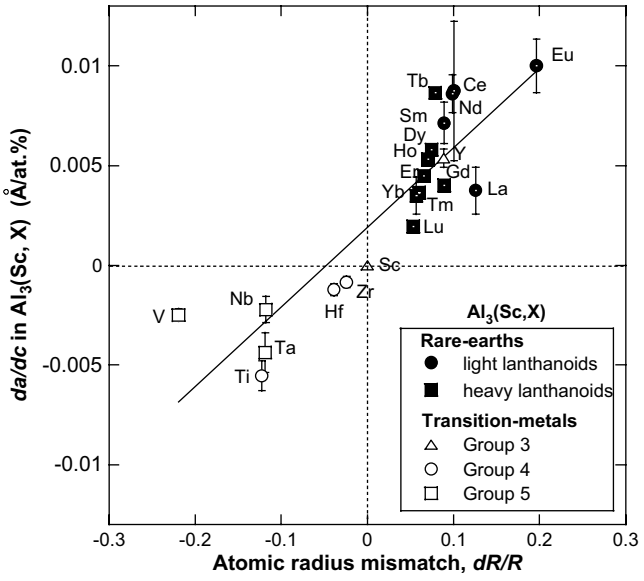

Fig. 7. Relationship between the atomic radius mismatch between elements X and Sc, dR/R, and the composition dependence of the lattice parameter, da/dc, of the $L1_2$-Al_3(Sc,X) phase, including present data and literature values for transition metals [3] and rare-earths [6–8].

The effectiveness of ternary additions on solid-solution hardening of Al_3Sc is quantified by the slope of the best-fit line, dHV/dc, in Fig. 8(b). This value is not calculated for the low-solubility light REs (La, Ce, Nd and Eu), because it is possible that a small volume fraction of a finely dispersed hard $D0_{19}$ or $C11_b$ second phase, not visible in the SEM micrographs (Figs. 1–3), may be increasing hardness by dispersion strengthening. These precipitates could be identified by transmission electron microscopy, which is beyond the scope of the present paper. Fig. 9 shows the correlation between the concentration dependence of micro-hardness, dHV/dc, and the lattice strain, da/dc, in ternary Al_3Sc. For the lanthanoids (Sm, Yb, and Lu, to which Y is added) and the transition metals from Group 4 (Ti, Zr, and Hf), a best-fit straight line is drawn and it shows a reasonable correlation, indicative of a first-order elastic interaction between dislocations and solute atoms. Correlation is less good, but still suggestive, for lower-solubility Group 5 transition metals (V, Nb, and Ta). Thus, it is clear that the lattice strain is not the only parameter controlling hardness, since the lines for the lanthanoids (including Y) and the Group 4 and Group 5 transition metals are clearly separated from each other in Fig. 9. Valence effects must be operative as well, as also suggested for $L1_2$-Ni_3Al alloys with ternary transition-metal additions [26].

In an earlier paper [4], we investigated the compressive creep behavior for $Al_3(Sc_{0.74}TM_{0.26})$, where TM is a transition metal from Group 3 (Y) or Group 4 (Ti, Zr, Hf). At 873 K, a decrease in creep rates of one order of magnitude was found for Zr and Hf, and two orders of magnitude for Ti and Y. These trends were in reasonably good agreement with the room temperature hardness of the alloys (HV = 1180–1570 MPa). The exact mechanism responsible for solid-solution strengthening at ambient and elevated temperatures must await precise observations of dislocations in indented or compressively deformed specimens, as many factors may be operating, e.g., interaction of solute atoms with vacancies and dislocation jogs, segregation on stacking faults and increase of the Peierls stress. Based on this correlation between ambient and elevated temperature strength, additions of Sm, Yb or Lu to Al_3Sc can be expected to improve very substantially the creep resistance of the ternary Al_3(Sc,RE) alloys, given their high hardness at ambient temperature (HV = 1670–2550 MPa, Fig. 8(b)).

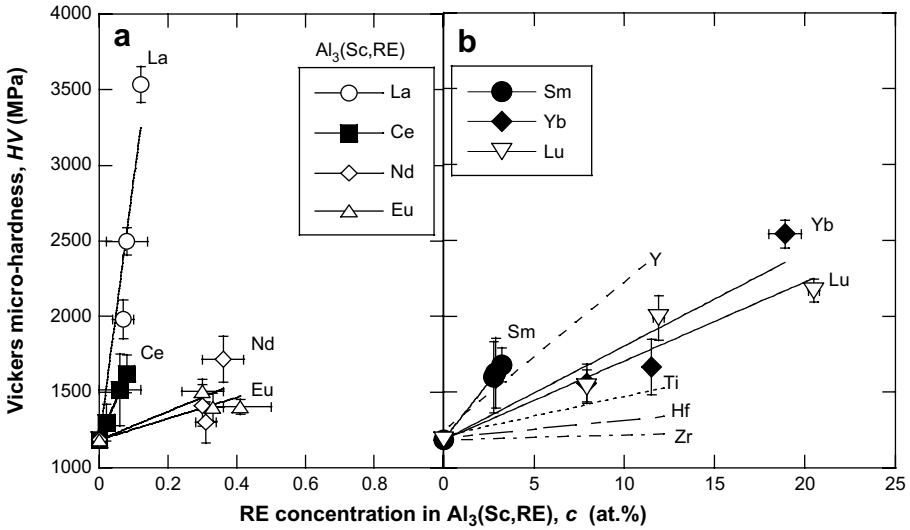

Fig. 8. Vickers micro-hardness of the $L1_2$-Al_3(Sc,RE) phase as a function of RE concentration in that phase.

3.5. Implications for Al–Sc alloy design

Coarse-grained, dilute Al–Sc alloys, consisting of an Al matrix strengthened by a low volume fraction of nano-size, coherent Al_3Sc precipitates, have excellent creep and coarsening resistance at elevated temperature (up to ~600 K) [27]. Ternary alloying additions to further improve their performances should have the following characteristics [27]: (1) show large solubility in $L1_2$-Al_3Sc, allowing replacement of expensive Sc; (2) maximize the volume fraction of precipitates, by extending rather than reducing the total solute (sum of Sc and RE) solubility in Al at elevated temperature; (3) have a low diffusion rate in Al, thus reducing precipitate coarsening; (4) increase (to maximize creep strength) or decrease (to minimize coarsening) the lattice parameter mismatch of Al_3Sc with Al; (5) reduce the Al_3Sc/Al interfacial energy to reduce coarsening and prevent loss of coherency; (6) strengthen the Al_3Sc precipitates to prevent their shearing by dislocations.

The previous and present research provided information on points (1), (4) and (6) as listed in Table 2. Concerning point (1), all elements in Table 2 (except the light RE elements La, Ce, Nd and Eu) have substantial solubility in $L1_2$-Al_3Sc. Concerning points (4), Y and all REs increase the lattice parameter of Al_3Sc and thus the mismatch with Al. In contrast, Group 4 and Group 5 transition metals (TM) reduce mismatch of Al_3Sc with Al. Thus simultaneous additions of RE and TM may allow to tailor mismatch while still reducing the amount of Sc used. Concerning point (6), Y, Sm, Yb and Lu are superior to Ti, Zr and Hf, and similar to V, Nb, and Ta (which have higher rates of hardening but lower solubility). Concerning point (3), the diffusivity of RE in Al is lower than Sc, but larger than for the TM, as reported in Ref. [27]; here again, simultaneous additions of both types of solutes may be optimal. Finally, the cost of heavy RE is superior to that of Group 4 and Group 5 transition metals, with the possible exception of Hf and Ta, but lower than that of Sc, making substitution of Sc with RE in these dilute Al–Sc alloys economically interesting [28].

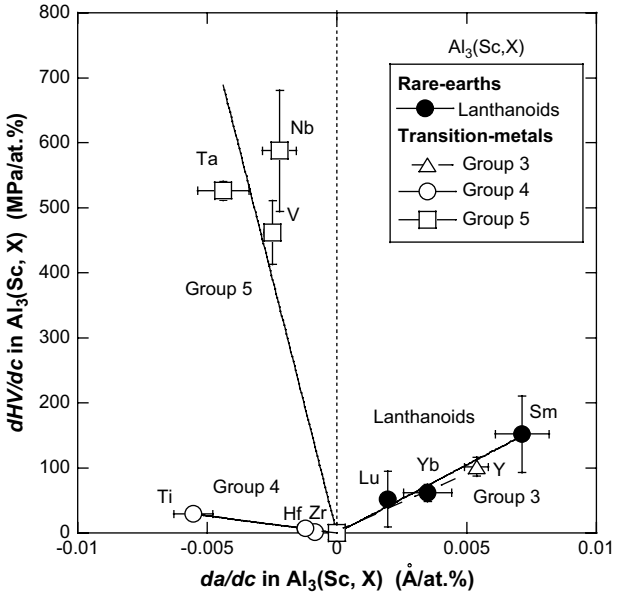

Fig. 9. Correlation between composition dependence of micro-hardness and concentration dependence of lattice parameter in the $L1_2$-Al_3(Sc,X) phase.

4. Conclusions

Ternary trialuminides $Al_3(Sc_{1-y}RE_y)$, where RE is one of the rare-earth elements La, Ce, Nd, Sm, Eu, Yb, and Lu, were investigated in the concentration range $0 \le y \le 0.75$. The following conclusions are drawn:

- Alloys containing light RE (La, Ce, Nd, Sm or Eu) consist of two phases with the $L1_2$-Al_3Sc and the $D0_{19}$-Al_3RE structures (except for Eu where the $D0_{19}$ phase is replaced by $C11_b$-Al_4Eu). Alloys with heavy RE (Yb or Lu) show a single $L1_2$-Al_3Sc phase.
- The maximum solubility in the $L1_2$-$Al_3(Sc_{1-y}RE_y)$ phase is 0.1 at.% ($y = 0.004$) for La and Ce, 0.4 at.% ($y = 0.016$) for Nd and Eu, and 3.2 at.% ($y = 0.128$) for Sm. The heavy REs (Yb and Lu) are fully soluble in the $L1_2$ phase. The solubility of Sc in the $D0_{19}$-Al_3RE phases varies between 0.7 and 9.2 at.% and is 0.5 at.% in $C11_b$-Al_4Eu.
- The lattice parameter of the $L1_2$-$Al_3(Sc_{1-y}RE_y)$ phase increases near linearly with increasing substitution of Sm, Yb or Lu, according to Vegard's law. The concentration dependence of the lattice parameter correlates with the atomic size mismatch between Sc and RE (for Sm, Yb and Lu studied here and other heavy REs reported in the literature).

Table 2
RE maximum solubility in $L1_2$-Al_3(Sc,RE) phase as well as lattice parameter, lattice mismatch with Al and micro-hardness at maximum solubility.

Element	Atomic number	Metallic radius[b] (Å)	Maximum solubility in Al_3Sc (%)	Lattice parameter of Al_3Sc at max. solubility (Å)	da/dc (Å/at.%) × 1000	Lattice mismatch of Al–Al_3Sc at max. solubility (%)	Maximum micro-hardness in Al_3Sc (MPa)	dHV/dc (MPa/at.%)	Ref.
Al	13	1.432	NA	4.049 (Al)	NA	NA	NA	NA	[3]
Sc	21	1.641	NA	4.103	NA	1.32	1190	NA	[3]
Ti	22	1.462	48	4.036	−5.5	0.32	1540	29.4	[3]
V	23	1.346	11	4.096	−2.5	1.15	2450[c]	461[c]	[3]
Y	39	1.801	46	4.164	5.4	2.76	2360	102	[3]
Zr	40	1.602	51	4.095	−0.8	1.12	1210	2.0	[3]
Nb	41	1.468	9	4.098	−2.2	1.20	3470[c]	588[c]	[3]
Hf	72	1.580	50	4.086	−1.2	0.90	1380	6.9	[3]
Ta	73	1.467	7	4.094	−4.4	1.10	2490[c]	529[c]	[3]
La	57	1.877	0.5	4.103	3.8	1.32	3540[c]	17 200[c]	[a]
Ce	58	1.825	0.3	4.103	8.8	1.32	1620[c]	5490[c]	[a]
Pr	59	1.828	–	–	–	–	–	–	
Nd	60	1.821	1	4.106	8.6	1.39	1720[c]	936[c]	[a]
Pm	61	1.810	–	–	–	–	–	–	
Sm	62	1.802	13	4.126	7.1	1.87	1680	152	[a][8]
Eu	63	2.042	2	4.106	10	1.39	1510[c]	702[c]	[a]
Gd	64	1.802	15	4.118	3.2	1.68	–	–	[7]
Tb	65	1.782	43	4.196	8.7	3.50	–	–	[6]
Dy	66	1.773	60	4.190	5.8	3.37	–	–	[6]
Ho	67	1.766	72	4.199	5.3	3.57	–	–	[6]
Er	68	1.757	100	4.160	4.5	2.67	–	–	[6]
Tm	69	1.746	100	4.194	3.6	3.46	–	–	[8]
Yb	70	1.740	100	4.169	5.7	2.88	2540	61.8	[a]
Lu	71	1.734	100	4.143	5.3	2.27	2170	52.1	[a] [8]

[a] Present study.
[b] Source – metallic hard-sphere radius [24].
[c] May be due to second phase effect.

- The Vickers micro-hardness of $L1_2$-$Al_3(Sc_{1-y}RE_y)$ increases linearly with increasing RE concentration for Sm, Yb or Lu. The concentration dependencies of hardness and lattice parameter are linearly correlated for Y, Sm, Yb and Lu. A similar, but less strong, dependency exists for Group 4 transition metals (Ti, Zr, and Hf).

Acknowledgments

DCD acknowledges the support of the US Department of Energy through grant DE-FG02-98ER45721.

References

[1] Schneibel JH, Hazzledine PM. J Mater Res 1992;7:868–75.
[2] Nakayama Y, Mabuchi H. Intermetallics 1993;1:41–8.
[3] Harada Y, Dunand DC. Mater Sci Eng 2002;A329–A331:686–95.
[4] Harada Y, Dunand DC. Acta Mater 2000;48:3477–87.
[5] Horovitz CT, Gschneidner KA, Melson GA, Youngblood DH, Schock HH. Scandium – its occurrence, chemistry, physics, metallurgy, biology and technology. Academic Press Inc.; 1975.
[6] Zalutska OI, Ryabov VR, Zalutskii II. Dopov Akad Nauk Ukr RSR A 1969;3:255–9.
[7] Zalutska OI, Kontsevii VG, Karamishev NI, Ryabov VR, Zalutskii II. Dopov Akad Nauk Ukr RSR A 1970;8:751–3.
[8] Zalutska OI, Cherkashin EE, Zalutsky II. Strukt. Faz, Fazovye Prevrashch. Diagr. Sostoyaniya Met. In: Ivanov OS, Alekseeva ZM, editors. Moscow: Sist. Publ. Nauka; 1974. p. 186–94.
[9] Fuller CB, Seidman DN, Dunand DC. Scr Mater 1999;40:691–6.
[10] Han BQ, Lavernia EJ, Mohamed FA. Metall Mater Trans A 2005;36:345–55.
[11] Royset J, Ryum N. Int Mater Rev 2005;50:19–44.
[12] Senkova SV, Senkov ON, Miracle DB. Metall Mater Trans A 2006;37:3569–75.
[13] Fuller C, Seidman DN, Dunand DC. Acta Mater 2003;51:4803–14.
[14] Seidman DN, Marquis EA, Dunand DC. Acta Mater 2002;50:4021–35.
[15] Marquis EA, Dunand DC. Scr Mater 2002;47:503–8.
[16] Sawtell RR, Morris JW. Dispersion strengthened aluminum alloys. Warrendale, PA: TMS; 1988. p. 409–20.
[17] Karnesky RA, Seidman DN, Dunand DC. Mater Sci Forum 2006;519–521:1035–40.
[18] Karnesky RA, Van Dalen ME, Dunand DC, Seidman DN. Scr Mater 2006;55:246–65.
[19] Van Dalen ME, Dunand DC, Seidman DN. J Mater Sci 2006;41:7814–23.
[20] Palenzon AJ. Less-Common Met 1972;29:289–92.
[21] George EP, Pope DP, Fu CL, Schneibel JH. ISIJ Int 1991;31:1063–75.
[22] The powder diffraction file and related products. Newtown Square, PA: ICDD; 2005.
[23] Denton AR, Ashcroft NW. Phys Rev A 1991;43:3161–4.
[24] Teatum ET, Gshneidner KA, Waber JT. Report of Los Alamos scientific laboratory of the University of California, LA-2345. Washington, DC: Department of Commerce; 1968.
[25] Yamamoto Y, Hashimoto K, Kimura T, Moriya H, Nobuki N, Kohno N. J Jpn Inst Met 1998;62:844–52.
[26] Mishima Y, Ochiai S, Yodokawa M, Suzuki T. Trans JIM 1986;27:41–50.
[27] Knipling KE, Dunand DC, Seidman DN. Z Metallkd 2006;97:246–65.
[28] Metal prices in the United States through 1998. Reston, VA: United States Geological Survey; 1998.